Inorg. Chem. **2006**, *45*, 2317–2326

Hexanuclear Iron(III) Salicylaldoximato Complexes Presenting the $[Fe_6(\mu_3\text{-}O)_2(\mu_2\text{-}OR)_2]^{12+}$ Core: Syntheses, Crystal Structures, and Spectroscopic and Magnetic Characterization

Catherine P. Raptopoulou,*,† Athanassios K. Boudalis,† Yiannis Sanakis,† Vassilis Psycharis,† Juan Modesto Clemente-Juan,‡ Michael Fardis,† George Diamantopoulos,† and George Papavassiliou†

Institute of Materials Science, NCSR "Demokritos", 15310 Aghia Paraskevi, Athens, Greece, and Instituto de Ciencia Molecular, Universidad de Valencia, c/ Doctor Moliner 50, 46100 Burjassot, Spain

Received November 10, 2005

The use of salicylaldehyde oxime (H_2salox) in iron(III) carboxylate chemistry has yielded two new hexanuclear compounds $[Fe_6(\mu_3\text{-}O)_2(O_2CPh)_{10}(salox)_2(L)_2]\cdot x$MeCN$\cdot y H_2O$ [L = $MeCONH_2$, $x = 6$, $y = 0$ (**1**); L = H_2O, $x = 2$, $y = 3$ (**2**)]. Compound **1** crystallizes in the triclinic space group $P\bar{1}$ with (at 25 °C) $a = 13.210(8)$ Å, $b = 13.87(1)$ Å, $c = 17.04(1)$ Å, $\alpha = 105.79(2)°$, $\beta = 96.72(2)°$, $\gamma = 116.69(2)°$, $V = 2578.17(2)$ Å^3, and $Z = 1$. Compound **2** crystallizes in the monoclinic space group $C2/c$ with (at 25 °C) $a = 21.81(1)$ Å, $b = 17.93(1)$ Å, $c = 27.72(1)$ Å, $\beta = 111.70(2)°$, $V = 10070(10)$ Å^3, and $Z = 4$. Complexes **1** and **2** contain the $[Fe_6(\mu_3\text{-}O)_2(\mu_2\text{-}OR)_2]^{12+}$ core and can be considered as two $[Fe_3(\mu_3\text{-}O)]$ triangular subunits linked by two μ_2-oximato O atoms of the salox^{2-} ligands, which show the less common $\mu_3{:}\eta^1{:}\eta^2{:}\eta^1$ coordination mode. The benzoato ligands are coordinated through the usual syn,syn-$\mu_2{:}\eta^1{:}\eta^1$ mode. The terminal $MeCONH_2$ ligand in **1** is the hydrolysis product of the acetonitrile solvent in the presence of the metal ions. Mössbauer spectra from powdered samples of **2** give rise to two well-resolved doublets with an average isomer shift consistent with that of high-spin Fe^{III} ions. The two doublets, at an approximate 1:2 ratio, are characterized by different quadrupole splittings and are assigned to the nonequivalent Fe^{III} ions of the cluster. Magnetic measurements of **2** in the 2–300 K temperature range reveal antiferromagnetic interactions between the Fe^{III} ions, stabilizing an $S = 0$ ground state. NMR relaxation data have been used to investigate the energy separation between the low-lying states, and the results are in agreement with the susceptibility data.

Introduction

Polynuclear 3d metal complexes have been extensively studied over the past years not only as valuable models for the study of biological systems[1] but also as molecular materials with promising properties (magnetic,[2] optical,[3] electronic,[4] catalytic,[5] etc) that are closely related to their structural characteristics. Thus, to exploit these properties, it is crucial to understand their origin and to be able to fine-tune them through synthetic modifications. To satisfy these demands, the most productive way so far has been the systematic exploration of the reaction conditions affecting the identity of the products. This, in other words, constitutes a "trial and error" method in which suitable modifications

* To whom correspondence should be addressed. E-mail: craptop@ims.demokritos.gr. Tel: +3210-6503365. Fax: +3210-6519430.

† NCSR "Demokritos".

‡ Universidad de Valencia.

(1) (a) Brechin, E. K.; Knapp, M. J.; Huffman, J. C.; Hendrickson, D. N.; Christou, G. *Inorg. Chim. Acta* **2000**, *297*, 389. (b) Lippard, S. J. *Angew. Chem., Int. Ed. Engl.* **1988**, *27*, 344. (c) Lippard, S. J.; Berg, J. M. *Principles of Bioinorganic Chemistry*; University Science Book: Mill Valley, CA, 1994. (d) Mishra, A.; Wernsdorfer, W.; Abboud, K. A.; Christou, G. *Chem. Commun.* **2005**, 54.

(2) For recent examples involving manganese and iron complexes, see: (a) Tasiopoulos, A. J.; Vinslava, A.; Wernsdorfer, W.; Abboud, K. A.; Christou, G. *Angew. Chem., Int. Ed.* **2004**, *43*, 2117. (b) Soler, M.; Wernsdorfer, W.; Folting, K.; Pink, M.; Christou, G. *J. Am. Chem. Soc.* **2004**, *126*, 2156. (c) Aliaga-Alcalde, N.; Edwards, R. S.; Hill, S. O.; Wernsdorfer, W.; Folting, K.; Christou, G. *J. Am. Chem. Soc.* **2004**, *126*, 12503. (d) Wang, S.; Zuo, J.-L.; Zhou, H.-C.; Choi, H. J.; Ke, Y.; Long, J. R.; You, X.-Z. *Angew. Chem., Int. Ed.* **2004**, *43*, 5940. (e) Oshio, H.; Hoshino, N.; Ito, T.; Nakano, M. *J. Am. Chem. Soc.* **2004**, *126*, 8805.

(3) (a) Niu, Y.; Song, Y.; Hou, H.; Zhu, Y. *Inorg.Chem.* **2005**, *44*, 2553. (b) Susumu, K.; Duncan, T. V.; Therien, M. J. *J. Am. Chem. Soc.* **2005**, *127*, 5186. (c) Meng, X.; Song, Y.; Hou, H.; Fan, Y.; Li, G.; Zhu, Y. *Inorg. Chem.* **2003**, *42*, 1306. (d) Tian, L.; Zhang, W.; Yang, B.; Lu, P.; Zhang, M.; Lu, D.; Ma, Y.; Shen, J. *J. Phys. Chem. B* **2005**, *109*, 6944. (e) Hou, H.; Wei, Y.; Song, Y.; Mi, L.; Tang, M.; Li, L.; Fan, Y. *Angew. Chem., Int. Ed*. **2005**, *44*, 6067.

10.1021/ic051945q CCC: $33.50
Published on Web 02/09/2006

of the reaction conditions lead to new molecular structures with optimized physical properties.[6,7] The experience gained in each step is used to design new synthetic routes, thus forming a positive feedback loop. However, at this moment we are still in the realm of serendipitous assembly as far as 3d cluster chemistry is concerned.[8] Therefore, more studies in this direction need to be carried out.

We have recently been interested in polynuclear metal clusters that may display single-molecule magnet (SMM) behavior both because of their potential technological applications[9] and because SMMs exhibit interesting physical and quantum phenomena previously predicted by theory.[10] To function as SMMs, the metal clusters should combine a large-spin ground state S and an Ising (or easy-axis) type of magnetization expressed by an axial zero-field splitting tensor with $D < 0$.[11] While it is easier to satisfy the first requirement by choosing metal ions with large spin values (e.g., Fe^{III} $S = {}^5/_2$, Mn^{III} $S = 2$, Mn^{IV} $S = {}^3/_2$, etc.) and suitable bridging ligands to promote high-spin ground states through suitable exchange interactions and spin topology, it is very difficult to satisfy the second requirement in a controllable way. Hence, a plethora of high-spin molecules do not display SMM behavior, and further studies need to be carried out by using new ligands or a combination of ligands in order to achieve this goal.

Our approach to the field concerns the investigation of the reaction between 3d metal ions and salicylaldehyde oxime (H_2salox) in the presence of carboxylates. H_2salox is a multifunctional ligand that in its mono- or dianionic form can adopt various coordination modes, giving rise to a number of homo- and heterometallic complexes.[12] We have recently reported[13] the first two members of a new class of SMMs containing exclusively Mn^{III} ions with blocking temperatures greater than 2 K, compounds $[Mn_6O_2(O_2CR)_2(salox)_6(EtOH)_4]$ [R = Me (**I**); Ph (**II**)], where $salox^{2-}$ adopts the rare μ_3:η^1:η^2:η^1 coordination mode, which usually leads to high-nuclearity complexes.[14] Expanding our research into iron(III) carboxylate chemistry, we have reported[15] the synthesis and structural, spectroscopic, and magnetic characterization of two neutral trinuclear oxo-centered ferric complexes, $[Fe_3(\mu_3\text{-}O)(O_2CPh)_5(salox)L^1L^2]$ [$L^1 = L^2 =$ MeOH (**III**); $L^1 =$ EtOH and $L^2 = H_2O$ (**IV**)]. In this case, the $salox^{2-}$ ligand adopts the common μ_2:η^1:η^2:η^1 coordination mode so the possibility of further use of the oximato O atom to bridge a second metal and to increase the nuclearity of the derived complex is present. By working in the weakly coordinating solvent MeCN, we isolated the hexanuclear complexes $[Fe_6(\mu_3\text{-}O)_2(O_2CPh)_{10}(salox)_2(L)_2]\cdot x$MeCN$\cdot y H_2O$ [L = $MeCONH_2$, $x = 6$, $y = 0$ (**1**); L = H_2O, $x = 2$, $y = 3$ (**2**)], which are studied structurally. **2** is additionally studied spectroscopically (^{57}Fe Mössbauer, solid-state NMR) and magnetically. Furthermore, in addition to the reaction pathways for the formation of **1** and **2**, we report a new reaction pathway to **III** and **IV**, to better map this reaction system. In both **1** and **2**, the $salox^{2-}$ ligand adopts the rare μ_3:η^1:η^2:η^1 coordination mode, leading to a topology of the six Fe^{III} ions analogous to that of the hexanuclear manganese(III) complexes **I** and **II** (other crystallographically established coordination modes of $Hsalox^-$ and $salox^{2-}$ have been reported by us elsewhere[15]).

Experimental Section

Materials. All manipulations were performed under aerobic conditions using materials as received (Aldrich Co.). All chemicals and solvents were reagent-grade. Basic iron(III) benzoate "$[Fe_3(\mu_3\text{-}O)(O_2CPh)_6(H_2O)_2(OH)]$" was synthesized as previously described.[16]

Physical Measurements. Elemental analysis for C, H, and N was performed on a Perkin-Elmer 2400/II automatic analyzer. IR spectra were recorded as KBr pellets in the range of 4000−400 cm^{-1} on a Bruker Equinox 55/S FT-IR spectrophotometer. Variable-temperature magnetic susceptibility measurements were carried out on polycrystalline samples of **2** in the 2.0−300 K temperature range using a Quantum Design MPMS SQUID susceptometer under a magnetic field of 1.5 T. Diamagnetic corrections for the complexes were estimated from Pascal's constants. The calculation of the magnetic susceptibility was accomplished using a modified version of MAGPACK.[17] Minimization was carried out with an adapted

(4) (a) Yu, G.; Yin, S.; Liu, Y.; Shuai, Z.; Zhu, D. *J. Am. Chem. Soc.* **2003**, *125*, 14816. (b) Bordiga, S.; Lamberti, C.; Ricchiardi, G.; Regli, L.; Bonino, F.; Damin, A.; Lillerud, K.-P.; Bjorgen, M.; Zecchina, A. *Chem. Commun.* **2004**, 2300. (c) Shi, J.-M.; Xu, W.; Liu, Q,-V.; Liu, F.-I.; Huang, Z.-I.; Lei, H.; Yu, W.-T.; Fang, Q. *Chem. Commun.* **2002**, 756. (d) Coronado, E.; Clemente-León, M.; Galán-Mascarós, J. R.; Giménez-Saiz, C.; Gómez-García, C. J.; Martínez-Ferrero, E. *J. Chem. Soc., Dalton Trans.* **2000**, 3955.

(5) For recent representative examples involving iron complexes, see: (a) Legros, J.; Bolm, C. *Chem.—Eur. J.* **2005**, *11*, 1086. (b) Avenier, F.; Dubois, L.; Dubourdeaux, P.; Latour, J.-M. *Chem. Commun*. **2005**, 480. (c) Bénisvy, L.; Chottard, J.-C.; Marrot, J.; Li, Y. *Eur. J. Inorg. Chem.* **2005**, 999.

(6) (a) Brockman, J. T.; Abboud, K. A.; Hendrickson, D. N.; Christou, G. *Polyhedron* **2003**, *22*, 1765. (b) Chakov, N. E.; Wernsdorfer, W.; Abboud, K. A.; Hendrickson, D. N.; Christou, G. *J. Chem. Soc., Dalton Trans*. **2003**, 2243. (c) Kuroda-Sowa, T.; Nogami, T.; Konaka, H.; Maekawa, M.; Munakata, M.; Miyasaka, H.; Yamashita, M. *Polyhedron* **2003**, *22*, 1795.

(7) (a) Tsohos, A.; Dionyssopoulou, S.; Raptopoulou, C. P.; Terzis, A.; Bakalbassis, E. G.; Perlepes, S. P. *Angew. Chem., Int. Ed.* **1999**, *38*, 983. (b) Papaefstathiou, G. S.; Perlepes, S. P.; Escuer, A.; Vicente, R.; Font-Bardia, M.; Solans, X. *Angew. Chem., Int. Ed.* **2001**, *40*, 884. (c) Boudalis, A. K.; Donnadieu, B.; Nastopoulos, V.; Clemente-Juan, J. M.; Mari, A.; Sanakis, Y.; Tuchagues, J. P.; Perlepes, S. P. *Angew. Chem., Int. Ed*. **2004**, *43*, 2266.

(8) Winpenny, R. E. W. *J. Chem. Soc., Dalton Trans* **2002**, 1.

(9) (a) Leuenberger, M. N.; Loss, D. *Nature* **2001**, *410*, 789. (b) Cavallini, M.; Gomez-Segura, J.; Ruiz-Molina, D.; Massi, M.; Albonetti, C.; Rovira, C.; Veciana, J.; Biscarini, F. *Angew. Chem., Int. Ed.* **2005**, *44*, 888.

(10) (a) Friedman, J. R.; Sarachik, M. P.; Tejada, J.; Ziolo, R. *Phys. Rev. Lett.* **1996**, *76*, 3830. (b) Thomas, L.; Lionti, F.; Ballou, R.; Gatteschi, D.; Sessoli, R.; Barbara, B. *Nature* **1996**, *383*, 145. (c) Gatteschi, D.; Sessoli, R.; *J. Magn. Magn. Mater*. **2004**, *272−276*, 1030.

(11) Christou, G.; Gatteschi, D.; Hendrickson, D. N.; Sessoli, R. *MRS Bull.* **2000**, *25*, 1.

(12) Chaudhuri, P. *Coord. Chem. Rev.* **2003**, *243*, 143.

(13) Milios, C. J.; Raptopoulou, C. P.; Terzis, A.; Lloret, F.; Vicente, R.; Perlepes, S. P.; Escuer, A. *Angew. Chem., Int. Ed.* **2004**, *43*, 210.

(14) (a) Thorpe, J. M.; Beddoes, R. L.; Collison, D.; Garner, C. D.; Helliwell, M.; Holmes, J. M.; Tasker, P. A. *Angew. Chem., Int. Ed.* **1999**, *38*, 1119. (b) Chaudhuri, P.; Hess, M.; Rentschler, E.; Weyhermüller, T.; Flörke, U. *New J. Chem.* **1998**, 553. (c) Zerbib, V.; Robert, F.; Gouzerh, P. *J. Chem. Soc., Chem. Commun.* **1994**, 2179.

(15) Raptopoulou, C. P.; Sanakis, Y.; Boudalis, A. K.; Psycharis, V. *Polyhedron* **2005**, *24*, 711.

(16) Earnshaw, A.; Figgis, B. N. *J. Chem. Soc. A* **1966**, 1656.

(17) (a) Borrás-Almenar, J. J.; Clemente-Juan, J. M.; Coronado, E.; Tsukerblat, B. S. *Inorg. Chem.* **1999**, *38*, 6081. (b) Borrás-Almenar, J. J.; Clemente-Juan, J. M.; Coronado, E.; Tsukerblat, B. S. *J. Comput. Chem*. **2001**, *22*, 985.

version of MINUIT.[18] The error factor R is defined as

$$R = \sum \frac{(x_{exp} - x_{calc})^2}{N x_{exp}^2}$$

where N is the number of experimental points. Mössbauer spectra were taken with a constant-acceleration spectrometer using a ^{57}Co (Rh) source at room temperature and a variable-temperature Oxford cryostat. ^{1}H-pulsed NMR experiments were collected on a Bruker MSL200 spectrometer operating at 4.7 T (200.1 MHz for ^{1}H NMR). An Oxford 1200 CF continuous-flow cryostat was employed for measurements in the range of 5−300 K. The T_1 spin−lattice relaxation time was obtained using the standard saturation technique.[19] The relaxation recovery, $M(t)$, was generally a nonexponential function, mainly because of the many proton-nonequivalent nuclei, and the relaxation data were fitted to a modified stretched exponential function of the form[20]

$$M(t) = M_0 \exp\left[-\frac{t}{T_1}\left(1 + \frac{t}{T_1}\right)^{n-1}\right]$$

In the short time regime, $t \ll T_1$, this model exhibits the desired single-exponential behavior and has a finite time derivative at the origin.

$$t = 0: \quad \exp\left[-\frac{t}{T_1}\left(1 + \frac{t}{T_1}\right)^{n-1}\right] \rightarrow \exp\left[-\frac{t}{T_1}\right]$$

In the long time regime, $t \gg T_1$, the model exhibits the limiting stretched-exponential behavior:

$$\exp\left[-\frac{t}{T_1}\left(1 + \frac{t}{T_1}\right)^{n-1}\right] \rightarrow \exp\left[-\left(\frac{t}{T_1}\right)^{n}\right]$$

Preparation of the Complexes. [Fe$_6$(μ_3-O)$_2$(O$_2$CPh)$_{10}$(salox)$_2$(MeCONH$_2$)$_2$]·6MeCN (1). $FeCl_3 \cdot 6H_2O$ (0.135 g, 0.50 mmol) was added to a refluxing solution of H_2salox (0.069 g, 0.50 mmol) and sodium benzoate (0.216 g, 1.50 mmol) in acetonitrile (20 mL). The color of the solution immediately turned to deep red. After 24 h of reflux, a small amount of brown precipitate was filtered off, and it was characterized as **1** by FT-IR spectroscopy. The deep-brown filtrate was sealed and left undisturbed for about 2 months. By that time, X-ray-quality red crystals of **1** had formed (yield: 0.02 g, ∼11%). The crystals of **1** were collected by filtration, washed with cold MeCN, and dried in vacuo. The resulting powder was analyzed as solvent-free. Anal. Calcd (found) for $C_{88}H_{70}Fe_6N_4O_{28}$: C, 53.75 (53.60); H, 3.59 (3.55); N, 2.85 (2.82).

[Fe$_6$(μ_3-O)$_2$(O$_2$CPh)$_{10}$(salox)$_2$(H$_2$O)$_2$]·2MeCN·3H$_2$O (2). Method A. Solid H_2salox (0.034 g, 0.25 mmol) was added to a refluxing solution of "[Fe_3(μ_3-O)(O$_2$CPh)$_6$(H$_2$O)$_2$(OH)]" (0.082 g, 0.085 mmol) in MeCN (30 mL). The color of the solution immediately turned from orange to deep brown. The reflux was stopped, and the solution was placed in a closed vessel. After 3 days, X-ray-quality red crystals had formed (yield: 0.064 g, ∼80%). The crystals were collected by filtration, washed with cold MeCN, and dried in vacuo. The resulting powder was analyzed as solvent-free. Anal. Calcd (found) for $C_{84}H_{64}Fe_6N_2O_{28}$: C, 53.54 (53.40); H, 3.42 (3.30); N, 1.49 (1.25).

(18) James, F.; Roos, M. MINUIT Program, a System for Function Minimization and Analysis of the Parameters Errors and Correlations. *Comput. Phys. Commun.* **1975**, *10*, 345.
(19) Fukushima, E.; Roeder, S. B. W. *Experimental Pulse NMR*; Addison-Wesley: Reading, MA, 1981.
(20) Peyron, M.; Pierens, G. K.; Lucas, A.; Hall, L. D.; Stewart, R. C. *J. Magn. Reson. A* **1996**, *118*, 214.

Table 1. Crystallographic Data for **1**·6MeCN and **2**·2MeCN·3H$_2$O

	1·6MeCN	**2**·2MeCN·3H$_2$O
formula	$C_{100}H_{88}Fe_6N_{10}O_{28}$	$C_{88}H_{76}Fe_6N_4O_{31}$
fw	2212.90	2020.63
space group	$P\bar{1}$	$C2/c$
T, °C	25	25
λ, Å	Mo Kα (0.710 73 Å)	Mo Kα (0.710 73 Å)
a, Å	13.210(8)	21.81(1)
b, Å	13.87(1)	17.93(1)
c, Å	17.04(1)	27.72(1)
α, deg	105.79(2)	
β, deg	96.72(2)	111.70(2)
γ, deg	116.69(2)	
V, Å^3	2578.17(2)	10070(10)
Z	1	4
$\rho_{calcd}/\rho_{measd}$, g cm^{-3}	1.425/1.41	1.333/1.32
μ(Mo Kα), mm^{-1}	0.902	0.917
R1[a]	0.0718[b]	0.0726[c]
wR2[a]	0.1876[b]	0.1759[c]

[a] $w = 1/[\sigma^2(F_o^2) + (aP)^2 + bP]$ and $P = (\max)F_o^2(0) + 2F_c^2)/3$. R1 = $\sum(|F_o| - |F_c|)/\sum(|F_o|)$ and wR2 = $\{\sum[w(F_o^2 - F_c^2)^2]/\sum[w(F_o^2)^2]\}^{1/2}$. [b] For 3922 reflections with $I > 2\sigma(I)$. [c] For 2607 reflections with $I > 2\sigma(I)$.

Method B. A quantity of **III** (0.042 g, 0.042 mmol) or **IV** (0.071 g, 0.071 mmol) was dissolved in MeCN (30 or 20 mL, respectively), and the resulting deep-brown solutions were refluxed for 5 h. The brown precipitates that formed were filtered off, washed with cold MeCN, dried in vacuo, and characterized as **2** by FT-IR spectroscopy. Characteristic IR data (cm^{-1}, KBr pellet): 1596, ν(C═N); 1552, $\nu_{as}(CO_2)$; 1406, $\nu_s(CO_2)$ [Δ = 146 cm^{-1}]; 1295, ν(N−O$_{ox}$); 482, $\nu_{as}(Fe_3O)$. Yield: 0.03 g, ∼75%.

[Fe$_3$(μ_3-O)(O$_2$CPh)$_5$(salox)(MeOH)$_2$] (III). H_2salox (0.068 g, 0.50 mmol) was added to a refluxing orange solution of "[Fe_3(μ_3-O)(O$_2$CPh)$_6$(H$_2$O)$_2$(OH)]" (0.164 g, 0.17 mmol) in MeOH (20 mL). The reflux was continued overnight, and small amounts of a black precipitate were filtered off. The resulting solution was left for slow evaporation, and after a period of 1 week, deep-brown needles formed and were filtered off, washed with cold MeOH, and dried in vacuo (yield: 0.13 g, ∼80%). Unit-cell determination of the needles identified them as complex **III** [a = 19.85(3) Å, b = 27.17(4) Å, c = 19.88(2) Å, β = 98.88(3)°, and V = 10590(10) Å^3].[15]

[Fe$_3$(μ_3-O)(O$_2$CPh)$_5$(salox)(EtOH)(H$_2$O)] (IV). H_2salox (0.068 g, 0.50 mmol) was added to a refluxing orange solution of "[Fe_3(μ_3-O)(O$_2$CPh)$_6$(H$_2$O)$_2$(OH)]" (0.164 g, 0.17 mmol) in EtOH (20 mL). The reflux was continued for 1 h more, and the deep-brown solution was left for slow evaporation. After a period of 2 weeks, deep-brown prismatic crystals formed and were filtered off, washed with cold MeOH, and dried in vacuo (yield: 0.12 g, ∼70%). Unit-cell determination of the crystals identified them as complex **IV** [a = 15.12(2) Å, b = 15.63(2) Å, c = 20.18(3) Å, β = 95.32(3)°, and V = 4750(10) Å^3].[15]

X-ray Crystallography. A red prismatic crystal of **1** (0.08 × 0.18 × 0.55 mm) and a red prismatic crystal of **2** (0.12 × 0.16 × 0.75 mm) were mounted in capillaries. Diffraction measurements were made on a Crystal Logic Dual Goniometer diffractometer using graphite-monochromated Mo Kα radiation. Significant crystal data and parameters for data collection are reported in Table 1. Unit-cell dimensions were determined and refined by using the angular settings of 25 automatically centered reflections in the range of 11° < 2θ < 23°. Three standard reflections, monitored every 97 reflections, showed less than 3% intensity fluctuation and no decay. Lorentz and polarization corrections were applied using Crystal Logic software. The structures were solved by direct methods using *SHELXS-86*[21] and refined by full-matrix least-squares techniques on F^2 with *SHELXL-97*.[22] In both structural cases, the crystals had poor diffraction ability (despite their sufficient size)

Scheme 1. Reaction Scheme for the Synthesis of Compounds **1**, **2**, **III**, and **IV**

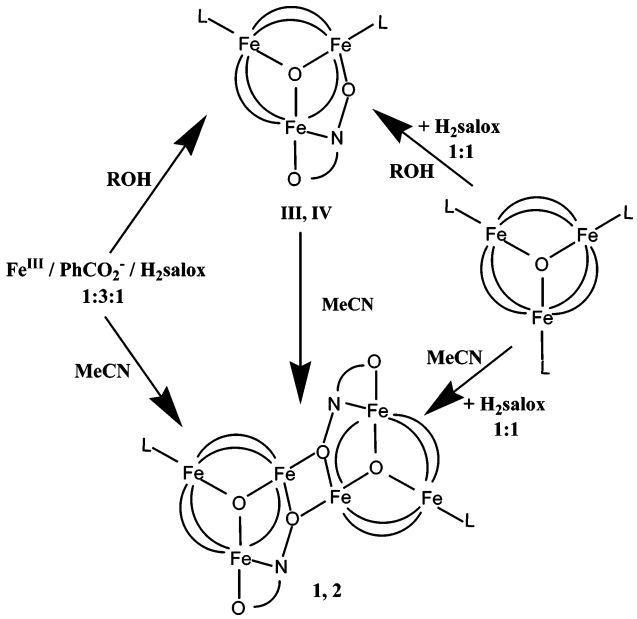

and the data were collected in increasing 2θ shells, and in each case, the data collection was terminated when about 50% of the collected shell data were unobserved. Nevertheless, the quality of the collected data was adequate to establish the structure of the complexes. Further experimental crystallographic details for **1**: $2\theta_{max} = 45°$; scan speed, 3.0°/min; scan range, $1.6 + \alpha_1\alpha_2$ separation; reflections collected/unique/used, 5494/5212 [$R_{int} = 0.0348$]/5212; 613 parameters refined; $(\Delta/\sigma)_{max} = 0.003$; $(\Delta\rho)_{max}/(\Delta\rho)_{min} = 0.657/-0.643$ e/Å^3; R/R_w (for all data), 0.0987/0.2161. H atoms were introduced at calculated positions as riding on bonded atoms. All non-H atoms were refined anisotropically, except those of the MeCN solvents, which were refined isotropically. The assignment of the terminal ligand $MeCONH_2$ instead of $MeCO_2H$ (which can be the final hydrolysis product of MeCN in the presence of metal ions) was based on H-bonding interactions between amide H atoms and the acetonitrile solvent molecules. Further experimental crystallographic details for **2**: $2\theta_{max} = 40°$, scan speed, 1.5°/min; scan range, $1.6 + \alpha_1\alpha_2$ separation; reflections collected/unique/used, 4667/4549 [$R_{int} = 0.0265$]/4549; 571 parameters refined; $(\Delta/\sigma)_{max} = 0.001$; $(\Delta\rho)_{max}/(\Delta\rho)_{min} = 0.558/-0.286$ e/Å^3; R/R_w (for all data), 0.1451/0.2175. H atoms were introduced at calculated positions as riding on bonded atoms. All non-H atoms were refined anisotropically, except those of the MeCN and H_2O solvents, which were refined isotropically.

Results and Discussion

Synthesis. Synthetic efforts to prepare polynuclear complexes in a more or less rational way have mainly led to two synthetic approaches. The first one concerns the in situ reaction of metal salts with suitable ligands, in ratios that favor the formation of polynuclear instead of mononuclear complexes, whereas the second one involves the use of small-nuclearity complexes, called "building blocks", to produce higher-nuclearity aggregates. In this work, we have employed both synthetic routes, which are shown in Scheme 1.

According to the first approach, the reaction of $Fe^{III}/PhCO_2^-/H_2$salox in a 1:3:1 respective molar ratio in alcoholic media has afforded the trinuclear oxo-centered compounds $[Fe_3(\mu_3\text{-}O)(O_2CPh)_5(salox)L^1L^2]$ [$L^1 = L^2 =$ MeOH (**III**); $L^1 =$ EtOH, $L^2 = H_2O$ (**IV**)].[15] In both complexes, the salox^{2-} ligand is coordinated through the common μ_2:η^1:η^1:η^1 mode, providing the possibility of further use of the oximato O atom to bind to a second metal and to increase the nuclearity of the derived complexes. By using the same reaction "blend" in the weakly coordinating acetonitrile, this possibility has been confirmed and the hexanuclear complex **1** has been isolated according to eq 1. In this case, it is assumed that the source of the O^{2-} ion is the H_2O from the starting material and/or the solvent.

$$6FeCl_3\cdot 6H_2O + 10PhCOONa + 2H_2salox \xrightarrow{MeCN} \underset{\mathbf{1}}{[Fe_6O_2(PhCO_2)_{10}(salox)_2(MeCONH_2)_2]} + 10NaCl + 8HCl + 34H_2O \quad (1)$$

The terminal $MeCONH_2$ ligand is the hydrolysis product of the acetonitrile solvent, which is favored in the presence of the metal ion.[23] The above reaction afforded compound **1** in very small quantities, making the study of its spectroscopic and magnetic properties impossible.

By following the "building block" synthetic approach, the 1:1 reaction between basic iron benzoate "$[Fe_3(\mu_3\text{-}O)(O_2CPh)_6(H_2O)_2(OH)]$" and H_2salox in MeCN has afforded the hexanuclear complex **2** in good yield, according to eq 2.

$$2[Fe_3O(O_2CPh)_6(H_2O)_2(OH)] + 2H_2salox \xrightarrow{MeCN} \underset{\mathbf{2}}{[Fe_6O_2(O_2CPh)_{10}(salox)_2(H2O)_2]} + 2HO_2CPh + 2H_2O \quad (2)$$

The same reaction mixture in alcoholic media has afforded the trinuclear compounds **III** and **IV**, whose identities have been proved by unit-cell determination.

From the molecular structures of compounds **III** and **IV**, it is evident that they might be used as "building blocks" themselves by using the oximato O atom of the salox^{2-} ligand to bind to a second metal, thus doubling the nuclearity of the complex. This possibility has been explored by dissolving compounds **III** and/or **IV** in acetonitrile. The brown precipitate formed was identified as compound **2** by FT-IR spectroscopy. Thus, it seems that, in the weakly coordinating MeCN, the apical coordination positions previously occupied by ROH in **III** and **IV** are now available for coordination by salox^{2-} and subsequent dimerization, thus increasing the nuclearity of the complex.

$$2[Fe_3O(O_2CPh)_5(salox)(EtOH)(H_2O)] \xrightarrow[\mathbf{IV}]{MeCN} \underset{\mathbf{2}}{[Fe_6O_2(O_2CPh)_{10}(salox)_2(H2O)_2]} + 2EtOH \quad (3)$$

In the IR spectrum of **1**, medium-intensity bands at 3063 and 2924 cm^{-1} are assigned to the $\nu(CH)_{aromatic}$ and $\nu(CH_3)$ stretching vibrations, respectively. A strong-intensity band at 1596 cm^{-1} and a medium-intensity band at 1292 cm^{-1}

(21) Sheldrick, G. M. *SHELXS-86: Structure Solving Program*; University of Göttingen: Göttingen, Germany, 1986.
(22) Sheldrick, G. M. *SHELXL-97: Crystal Structure Refinement*; University of Göttingen: Göttingen, Germany, 1997.

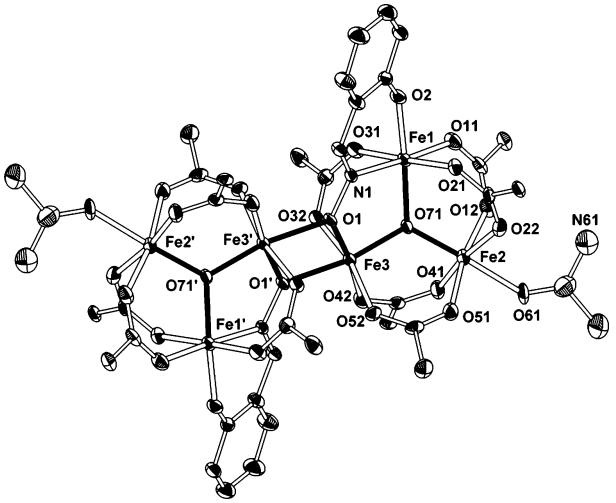

Figure 1. Partially labeled ORTEP plot of **1** with ellipsoids drawn at the 30% probability level. For clarity, H atoms and phenyl rings have been omitted. Primed atoms are generated by symmetry ($' = -x + 1, -y + 1, -z$).

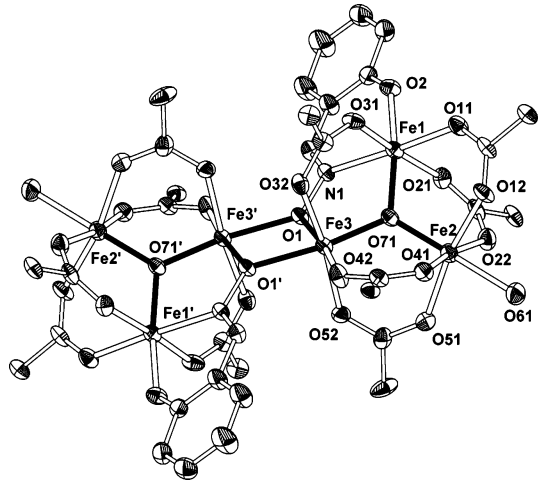

Figure 2. Partially labeled ORTEP plot of **2** with ellipsoids drawn at the 30% probability level. For clarity, H atoms and phenyl rings have been omitted. Primed atoms are generated by symmetry ($' = 0.5 - x, 1.5 - y, 1 - z$).

are assigned to the ν(C···N) and ν(N−O_{ox}) vibrations of the salicylaldoximato ligand, respectively.[24] The frequencies of the $\nu_{as}(CO_2)$ and $\nu_s(CO_2)$ bands of $PhCO_2^-$ at 1555 and 1408 cm^{-1}, respectively, differ by 147 cm^{-1}, less than that of NaO_2CPh (184 cm^{-1}), as expected for the bridging modes of benzoate ligation.[25] The two bands at 3365 and 3186 cm^{-1} are assigned to the NH stretching modes of the H-bonded NH_2 group of the terminal $MeCONH_2$, while the carbonyl absorption (amide I band) is observed at 1659 cm^{-1}.[26] A medium-intensity band at 480 cm^{-1} in the spectrum of **1** is characteristic of the presence of the [Fe_3O] moiety in the structure. In the IR spectrum of **2**, medium-intensity bands at 3409 and 3063 cm^{-1} are attributed to the $\nu(OH)_{H_2O}$ and $\nu(CH)_{aromatic}$ vibrations, respectively. A strong-intensity band at 1597 cm^{-1} and a medium-intensity band at 1295 cm^{-1} are assigned to the ν(C···N) and ν(N−O_{ox}) vibrations of the salicylaldoximato ligand. The frequencies of the $\nu_{as}(CO_2)$ and $\nu_s(CO_2)$ bands of $PhCO_2^-$ are observed at 1552 and 1407 cm^{-1} (Δ = 145 cm^{-1}), respectively. Finally, a medium-intensity band at 482 cm^{-1} is assigned to the $\upsilon_{as}(Fe_3O)$ vibration. In the IR spectra of both **1** and **2**, it is characteristic that the ν(N−O_{ox}) vibration of the salicylaldoximato ligand is observed at higher frequency with respect to **III** and **IV**, as a result of the μ_3:η^1:η^2:η^1 coordination mode in the hexanuclear complexes versus the μ_2:η^1:η^1:η^1 coordination mode in the trinuclear ones.

Description of the Structures. Compound **1** crystallizes in the triclinic space group $P\bar{1}$, and compound **2** crystallizes in the monoclinic space group $C2/c$. The molecular structures of **1** and **2** are given in Figures 1 and 2, respectively, and selected bond distances and angles for **2** are listed in Table 2 (the corresponding table, Table S1, for compound **1** is given in the Supporting Information). Both compounds contain the $[Fe_6(\mu_3\text{-}O)_2(\mu_2\text{-}OR)_2]^{12+}$ core, whose topology consists of six Fe^{III} ions arranged as two centrosymmetrically related [Fe_3-(μ_3-O)] subunits bridged by two oximato O atoms (O1 and O1′). The structure of each triangular [$Fe_3(\mu_3$-O)] subunit is quite similar to that of the precursor trinuclear compounds **III** and **IV**. There are two pairs, Fe1/Fe2 and Fe2/Fe3, which are bridged through one μ_2-oxide and two μ_2-benzoato ligands, while the pair Fe1/Fe3 is bridged by one μ_2-oxide, one μ_2-benzoato, and the oximato ligand. The sixth coordination position on Fe3, occupied by a terminal monodentate ligand in the trinuclear **III** and **IV**, is in the case of **1** and **2** occupied by a μ_2-oximato O atom belonging to the centrosymmetrically related [$Fe_3(\mu_3$-O)] subunit, thus increasing the nuclearity of the derived complex. The structure of complex **2** will be discussed in detail because compounds **1** and **2** have almost identical structures. The three Fe^{III} ions in each [$Fe_3(\mu_3$-O)] subunit form an almost isosceles triangle (see Table 2), and the closest Fe···Fe distance between the two [$Fe_3(\mu_3$-O)] subunits is 3.274(5) Å. The Fe−O_{ox} bond distances are in the range of 1.884−1.928 Å, and the [Fe_3-(μ_3-O)] subunit is planar. Ions Fe2 and Fe3 have an octahedral O-rich coordination environment, while Fe1 has a distorted octahedral O_5N coordination geometry. The two salicylaldoximato ligands adopt the rare μ_3:η^1:η^2:η^1 coordination mode, which has not only been observed in **I** and **II**[13] and in $[M^{III}_6(\mu_3\text{-}O)_2(salox)_6(\mu_2\text{-}O_2CR)_2(OH_2)_2(RCN)_2]$ (M = V^{III}, Cr^{III}, Mn^{III}, Fe^{III}, RCO_2^- = $Ph_3CCO_2^-$, $Me_3CCO_2^-$, $Ph_2C(OH)CO_2^-$, $PhCO_2^-$, $C_2H_5CO_2^-$)[12] but also in trinuclear and tetranuclear complexes.[14] The Fe−$O_{oximato}$ bond distances are 2.025 and 2.099 Å for the chelating and bridging modes, respectively. The Fe−$O_{phenoxy}$ and Fe−$N_{oximato}$ bond lengths are 1.914 and 2.156 Å, respectively. The whole salicylaldoximato ligand is planar and forms an angle of 44.2° with the [$Fe_3(\mu_3$-O)] plane. The benzoato ligands are coordinated in the common syn,syn-μ_2:η^1:η^1 mode, and the Fe−$O_{carboxylato}$ bond distances are in the range of 1.991−2.057 Å. Although

(23) Constable, E. C. *Metals and Ligand Reactivity*; VCH Publishers: New York, 1996; pp 65−72.
(24) Alexiou, M.; Dendrinou-Samara, C.; Raptopoulou, C. P.; Terzis, A.; Kessissoglou, D. P. *Inorg. Chem.* **2002**, *41*, 4732.
(25) Deacon, G. B.; Phillips, R. J. *Coord. Chem. Rev.* **1980**, *33*, 227.
(26) Bellamy, L. J. *The Infrared Spectra of Complex Molecules*; Chapman and Hall: London, 1975.

Table 2. Selected Bond Distances (Å) and Angles (deg) in **2**·2MeCN·3H$_2$O[a]

		Distances			
Fe1−O2	1.914(9)	Fe2−O71	1.867(8)	Fe3−O71	1.884(7)
Fe1−O71	1.928(8)	Fe2−O51	2.017(10)	Fe3−O42	2.004(9)
Fe1−O31	2.040(9)	Fe2−O41	2.044(10)	Fe3−O32	2.013(9)
Fe1−O11	2.023(9)	Fe2−O12	1.991(9)	Fe3−O52	1.999(9)
Fe1−O21	2.057(10)	Fe2−O22	2.018(10)	Fe3−O1	2.025(7)
Fe1−N1	2.156(10)	Fe2−O61	2.116(9)	Fe3−O1′	2.099(7)
Fe1···Fe2	3.301(5)	Fe1···Fe3	3.274(5)	Fe2···Fe3	3.260(5)
Fe3···Fe3′	3.274(5)				
		Angles			
O2−Fe1−O71	169.7(4)	O71−Fe2−O51	95.2(4)	O71−Fe3−O42	96.2(4)
O2−Fe1−O31	93.8(4)	O71−Fe2−O41	95.6(4)	O71−Fe3−O32	92.2(4)
O71−Fe1−O31	89.0(3)	O51−Fe2−O41	91.4(4)	O42−Fe3−O32	84.7(4)
O2−Fe1−O11	92.3(4)	O71−Fe2−O12	95.4(4)	O71−Fe3−O52	95.6(4)
O71−Fe1−O11	97.8(3)	O51−Fe2−O12	169.4(4)	O42−Fe3−O52	88.4(4)
O31−Fe1−O11	86.8(4)	O41−Fe2−O(12)	86.9(4)	O32−Fe3−O52	170.1(4)
O2−Fe1−O21	87.3(4)	O71−Fe2−O22	94.8(4)	O71−Fe3−O1	90.3(3)
O71−Fe1−O21	90.8(4)	O51−Fe2−O22	89.8(4)	O42−Fe3−O1	173.0(4)
O31−Fe1−O21	174.5(4)	O41−Fe2−O22	169.4(4)	O32−Fe3−O1	92.4(3)
O11−Fe1−O21	87.8(4)	O12−Fe2−O22	90.0(4)	O52−Fe3−O1	93.7(3)
O2−Fe1−N1	85.0(4)	O71−Fe2−O61	179.1(4)	O71−Fe3−O1′	165.2(3)
O71−Fe1−N1	85.0(4)	O51−Fe2−O61	85.0(4)	O42−Fe3−O1′	98.5(3)
O31−Fe1−N1	92.9(4)	O41−Fe2−O61	83.6(4)	O32−Fe3−O1′	87.5(3)
O11−Fe1−N1	177.2(4)	O12−Fe2−O61	84.4(4)	O52−Fe3−O1′	86.6(4)
O21−Fe1−N1	92.6(4)	O22−Fe2−O61	86.1(4)	O1−Fe3−O1′	74.9(3)
Fe1−O71−Fe2	120.9(4)	Fe1−O71−Fe3	118.4(4)	Fe2−O71−Fe3	120.7(4)
Fe3−O1−Fe3′	105.1(3)				

[a] Symmetry transformations used to generate equivalent atoms: ′ = 0.5 − *x*, 1.5 − *y*, 1 − *z*.

Table 3. Structural Characteristics of the Triangular [M$_3$(μ_3-O)] Unit in Compounds **2** and **I**−**IV**

	2[a]	**I**[b]	**II**[b,c]	**III**[a,c]	**IV**[a]
		Distances (Å)			
M1···M3	3.274	3.163	3.157	3.253	3.199
M1···M2	3.301	3.258	3.253	3.222	3.298
M2···M3	3.260	3.245	3.262	3.267	3.269
		Angles (deg)			
M1−O−M3	118.4	115.0	115.3	116.0	117.2
M1−O−M2	120.9	121.1	120.5	121.9	119.3
M2−O−M3	120.7	120.0	120.5	121.7	123.2

[a] M = Fe^{III}. [b] M = Mn^{III}. [c] Average values of the two crystallographically independent molecules in the asymmetric unit.

Chart 1. Schematic Diagram of Structures of **I** and **II**

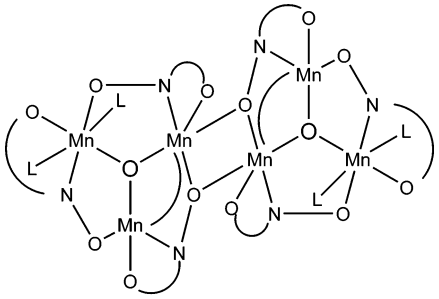

I, **II**

similar, compounds **1** and **2** present different lattice structures because of H-bonding interactions. In **1,** the amide H atoms of the MeCONH$_2$ ligands are H-bonded to the acetonitrile solvent molecules, leading to the formation of 1D polymeric chains (Figure S1 in the Supporting Information). On the other hand, no intermolecular H-bonding interactions are observed between the hexanuclear complexes in **2**, leading to isolated species in the crystal lattice.

A comparison of the structural characteristics of the triangular [Fe$_3$(μ_3-O)] subunit in complex **2** with those of the precursor trinuclear complexes **III** and **IV** (for a graphical representation, see Scheme 1) shows equivalent trends for the interatomic distances and angles between the Fe^{III} ions in terms of the types of bridging interactions (Table 3). In all three complexes, in the Fe1/Fe3 pair, bridged by one μ_2-oxide, one μ_2-benzoato, and one oximato bridge, a ∼3.26-Å separation is observed between the ferric ions, while the Fe−O−Fe angle of ∼117° is the smallest one in the triangular unit. On the other hand, in the Fe1/Fe2 and Fe2/Fe3 pairs, bridged by one μ_2-oxide and two μ_2-benzoato ligands, the Fe···Fe distances are differentiated (Fe1···Fe2 ∼3.32 Å; Fe2···Fe3 ∼ 3.27 Å) despite the similar Fe−O−Fe angles (∼121°). Moreover, the approach of a second triangular [Fe$_3$(μ_3-O)] subunit in the hexanuclear complex **2** at ca. 3.3 Å does not seem to affect the structural characteristics of the [Fe$_3$(μ_3-O)] triangle itself.

A comparison of the structural characteristics of the triangular [M$_3$(μ_3-O)] subunit in the hexairon complex **2** with those in **I** and **II** is also very interesting (for a graphical representation of **I** and **II**, see Chart 1). The metal ion topology in the three compounds is exactly the same, despite the different bridging modes observed in the triangular subunits. In the cases of **I** and **II**, there are two pairs, Mn1/Mn2 and Mn2/Mn3, bridged by one μ_2-oxide and one oximato group, and one pair, Mn1/Mn3, which is bridged by one μ_2-oxide, one μ_2-carboxylato, and one oximato group. In the latter pair, the Mn^{III} ions are separated by ∼3.16 Å and the Mn−O−Mn angle is ∼115°, values which are the smallest ones within the triangular subunit. The same trends, i.e., the smallest metal−metal interatomic distance and the largest deviation of the M−O−M angle from the ideal 120° value, are also observed in the ferric complex **2**. In the two former pairs, the Mn···Mn separations are almost identical (∼3.25 Å) and the Mn−O−Mn angles are ∼120°. The same

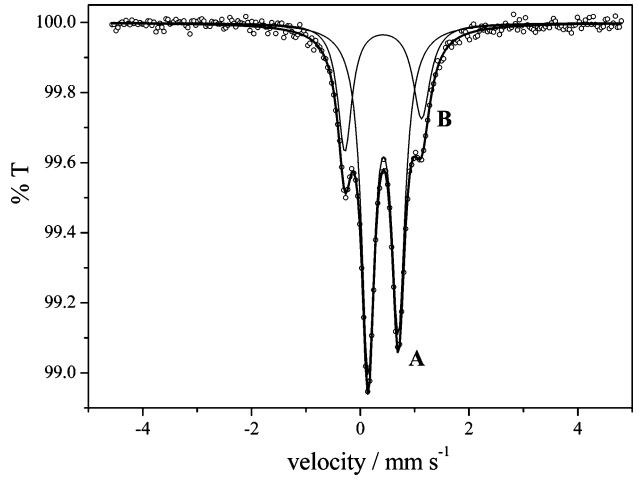

Figure 3. Mössbauer spectrum from a powdered sample of **2** at 295 K. Solid lines represent theoretical simulations assuming two doublets, **A** and **B**, with the parameters quoted in Table 4.

Table 4. Mössbauer Parameters for Complex **2**

iron site	T (K)	δ (mm s^{-1})	ΔE_Q (mm s^{-1})	$\Gamma_{1/2}$ (mm s^{-1})[a]
A (FeO_6)	295	0.43(1)	0.55(1)	0.13/0.14
B (FeO_5N)	295	0.43(1)	1.36(1)	0.16/0.22
A (FeO_6)	77	0.53(1)	0.62(1)	0.15/0.17
B (FeO_5N)	77	0.53(1)	1.23(1)	0.17/0.22
A (FeO_6)	4.2	0.53(1)	0.64(1)	0.16/0.17
B (FeO_5N)	4.2	0.54(1)	1.27(1)	0.18/0.19

[a] $\Gamma_{1/2}$ values for the left and right lines. The doublets are given as Γ_L/Γ_R.

trend is true for the Fe−O−Fe angles in **2**, but the Fe···Fe distances are substantially differentiated (~3.27 Å). Overall, the triangular subunits in **2**, **I**, and **II** are best described as isosceles triangles, where in **2** the base defined by Fe1/Fe2 is directed toward the outside of the hexanuclear core while in **I** and **II** the corresponding base defined by Mn1/Mn3 is directed toward the inside of the hexanuclear core.

Mössbauer Spectroscopy. Mössbauer spectra from powdered samples of **2** were collected between 4.2 and 295 K. These consist of two well-resolved quadrupole-split doublets (sites **A** and **B**) with Mössbauer parameters typical of high-spin Fe^{III} in octahedral O/N environments. A characteristic Mössbauer spectrum at 295 K is shown in Figure 3. Fairly narrow lines are observed, indicating a large degree of structural homogeneity. The asymmetry is attributed to alignment of the crystallites in the sample holder. The doublets exhibit similar isomer shifts but quite different quadrupole splittings ($\Delta E_{QA} < \Delta E_{QB}$), which is indicative of significant differences in the homogeneity and/or geometry of the coordination spheres.

The spectra can be simulated by assuming a 2:1 ratio for doublets **A** and **B**, respectively. The derived Mössbauer parameters are presented in Table 4. An increase of the isomer shift upon cooling is attributed to a second-order Doppler effect.[27]

Examination of the structure reveals that Fe1 exhibits an O_5N donor atom set, whereas Fe2 and Fe3 exhibit homogeneous O_6 donor atom sets. On the other hand, the bond lengths span the ranges 1.914−2.156 Å for Fe1, 1.867−2.116 Å for Fe2, and 1.884−2.099 Å for Fe3. Thus, Fe1 and Fe2 are characterized by a less symmetric environment than Fe3. These two competing factors should affect the electron-field gradient around the iron nuclei and, therefore, the quadrupole splittings. From the relative area of the two sites, the most reasonable assignment is that the minority doublet **B** is due to Fe1 whereas doublet **A**, representing the majority of the species, is assignable to both Fe2 and Fe3. The conclusion, therefore, is that ligand inhomogeneity is more influential to the quadrupole splitting than geometrical distortion. The same conclusion was drawn for complexes **III** and **IV** previously studied.[15] We note here the similarity of the spectra between complexes **2**, **III**, and **IV**, which all exhibit two doublets at a 2:1 ratio. Small albeit discernible differences for the ΔE_Q values of sites **A** and **B** in the three complexes can be identified.

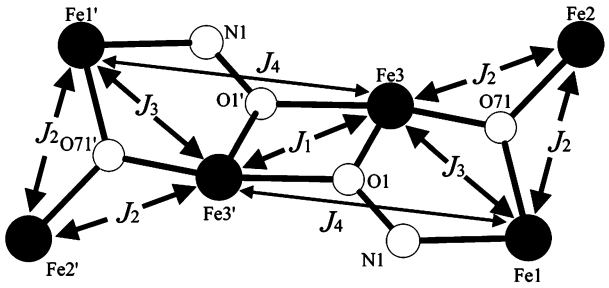

Figure 4. Exchange-interaction pattern for complex **2**.

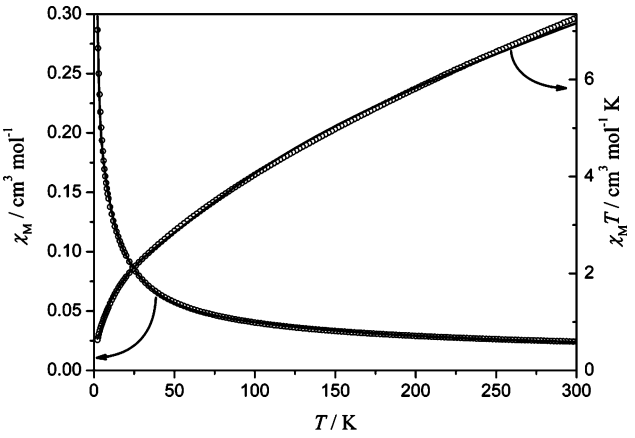

Figure 5. χ_M vs T and $\chi_M T$ vs T experimental data for complex **2** and the theoretical curve based on the Hamiltonian of eq 4 (solution a).

Magnetic Susceptibility Studies. The $\chi_M T$ product of **2** at 300 K is 7.27 cm^3 mol^{-1} K, significantly lower than the theoretically expected value for six noninteracting $S = {}^5/_2$ ions (26.28 cm^3 mol^{-1} K), indicating antiferromagnetic interactions (Figure 5). This is corroborated by the constant drop of the $\chi_M T$ product upon cooling, reaching a value of 0.63 cm^3 mol^{-1} K at 2.2 K. The magnetic susceptibility, χ_M, shows a constant increase upon cooling, which may be associated with a number of factors such as a magnetic ground state, low-lying magnetic excited states, or paramagnetic impurities. This will be analyzed in detail below.

Consideration of the molecular geometry (Figure 4) would suggest that five exchange parameters have to be taken into

(27) Greenwood, N. N.; Gibb, T. C. *Mössbauer Spectroscopy*; Chapman and Hall: London, 1971; pp 148−164.

account in order to describe the magnetic behavior of **2**: $J_A = J_{33'}$, $J_B = J_{23} = J_{2'3'}$, $J_C = J_{12} = J_{1'2'}$, $J_D = J_{13} = J_{1'3'}$ and $J_E = J_{13'} = J_{1'3}$. However, a closer inspection of the molecular structure allows for simplifications by considering the following: (i) the Fe1/Fe2 and Fe2/Fe3 pairs are bridged by one μ_2-oxide and two μ_2-benzoates; the Fe1/Fe3 pair is bridged by one μ_2-oxide, one μ_2-benzoato, and one oximato bridge; (ii) the Fe−O−Fe angles for the Fe1/Fe2, Fe2/Fe3, and Fe1/Fe3 pairs, which define the main superexchange pathways between ferric ions, are 120.95, 120.70, and 118.35°, respectively; (iii) atoms Fe1 and Fe3 of the Fe1/Fe2/Fe3 triangle both participate in interactions with atoms outside the triangle (Fe3′ and Fe1′/Fe3′, respectively), whereas atom Fe2 is the only one that does not; Fe2 can be considered the apex of an isosceles triangle with side Fe1/Fe3 as its base. Because of i−iii, interactions J_B and J_C are grouped together.

Thus, we can consider $J_A = J_1$, $J_B = J_C = J_2$, $J_D = J_3$, and $J_E = J_4$. The corresponding Hamiltonian is

$$\hat{H} = -2[J_1\hat{S}_3\hat{S}_{3'} + J_2(\hat{S}_1\hat{S}_2 + \hat{S}_2\hat{S}_3 + \hat{S}_{1'}\hat{S}_{2'} + \hat{S}_{2'}\hat{S}_{3'}) + J_3 (\hat{S}_1\hat{S}_3 + \hat{S}_{1'}\hat{S}_{3'}) + J_4(\hat{S}_1\hat{S}_{3'} + \hat{S}_{1'}\hat{S}_3)] \quad (4)$$

Because of the relatively large number of fitting parameters, initial fitting attempts were carried out by considering certain simplifications to verify that the problem is not overparametrized. Exchange interaction J_4 is expected to be the weakest one because of the large Fe1···Fe3′ separation and because the magnetic interaction is mediated by a diatomic oximato bridge. In addition, J_2 and J_3 are expected, on the basis of structural data, to be close in strength. Initial fitting attempts were carried out by considering $J_4 = 0$ and $J_2 = J_3$; however, these failed to yield an acceptable fit. Releasing only one of these two constraints resulted in marginal improvements. It was, therefore, decided that all four exchange interactions are necessary for the interpretation of the magnetic susceptibility data, with $J_4 \neq 0$ and $J_2 \neq J_3$.

With those considerations, the best-fit parameters were $J_1 = -19.7$ cm^{-1}, $J_2 = -35.8$ cm^{-1}, $J_3 = -63.8$ cm^{-1}, $J_4 = -4.99$ cm^{-1}, $g = 2.07$, with $R = 1.3 \times 10^{-4}$. One can deduce from these results that J_4 is indeed very weak, as expected, and that g is close to 2.0, which is reasonable for high-spin ferric ions. The ground state is characterized by $S = 0$. The first excited states are only 1.0 cm^{-1} ($S = 1$) and 10.0 cm^{-1} ($S = 2$) higher than the ground state, thus contributing to the magnetic susceptibility, because of their thermal population even at 2 K (Figure S2 in the Supporting Information).

A point that we thought of as worth exploring concerns the structural relationship of the complex with triangular basic iron carboxylates (see Description of the Structures). The magnetic properties of those are normally interpreted through a 2J model, considering an equilateral triangle, in which interactions along the sides of the triangle are associated with a parameter J and those along its base with a parameter J'. It is common for those[28] to present two best-fit solutions, one with $|J| > |J'|$ and one with $|J| < |J'|$. We, therefore, wondered if there could be a second solution with different relative strengths of J_2 and J_3, within the isosceles triangle Fe1/Fe2/Fe3. For that reason, the parameter space of J_2 and J_3 was explored by keeping J_1 and J_4 fixed to their previously defined values, and an error contour plot of J_2 vs J_3 was drawn (Figure 6). This verified the minimum previously mentioned (**a**) and revealed a second one (**b**) at $J_2 \sim -30$ cm^{-1} and $J_3 \sim -20$ cm^{-1}. Using those as initial conditions and by the release of J_1 and J_4, a second solution was obtained, with parameters $J_1 = -15.0$ cm^{-1}, $J_2 = -38.2$ cm^{-1}, $J_3 = -19.9$ cm^{-1}, $J_4 = -0.2$ cm^{-1}, $g = 2.08$, with $R = 2.8 \times 10^{-3}$ (solution **b′**). We observe that the relative strengths have now been inversed, like in basic iron carboxylates, with J_2 being stronger. However, the quality of this fit is inferior; thus, this solution is ruled out. Another observation is that no minimum is found for $J_2 = J_3$, which justifies our fitting strategy by which this constraint was abolished.

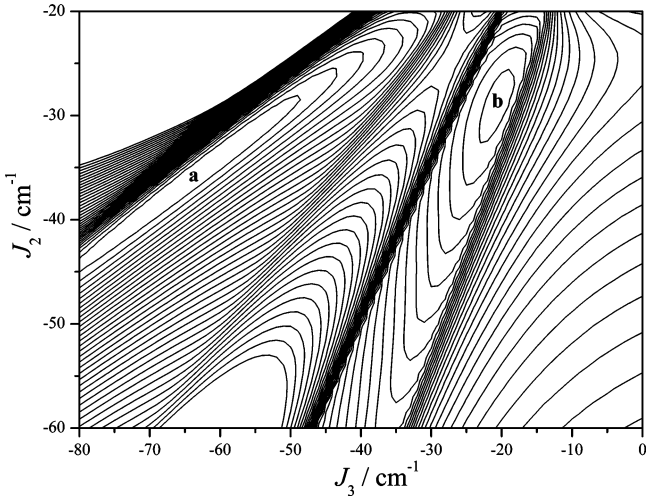

Figure 6. Surface error plot of J_2 vs J_3 (with $g = 2.00$) revealing the minima **a** and **b** for $|J_3| > |J_2|$ and $|J_3| < |J_2|$, respectively.

As a general conclusion, therefore, we may say that the complex retains some of the magnetic properties of simple basic iron carboxylates, which are, however, severely distorted because of the interaction of two triangular units. Specifically, although there are solutions for two pairs of J_2/J_3 values, only one is satisfactory, unlike basic iron carboxylates in which both are close in quality. In addition, although the overall coupling is antiferromagnetic in both types of complexes, the odd number of spins in Fe_3 clusters leads to half-integer spin systems (usually $S = {}^1/_2$), whereas the even number of spins in **2** leads to an integer spin system with $S = 0$.

These results can be compared to a series of studies carried out on hexanuclear ferric complexes containing two magnetically coupled [$Fe_3(\mu_3$-O)] triangular cores. It has been shown that the spin of the ground state can greatly vary depending on the coupling scheme and the relative strengths of the coupling constants. In one such case,[29] complexes [Fe_6O_2-

(28) Boudalis, A. K.; Sanakis, Y.; Raptopoulou, C. P.; Terzis, A.; Tuchagues, J.-P.; Perlepes, S. P. *Polyhderon* **2005**, *24*, 1540.

(29) Christmas, C. A.; Tsai, H.-L.; Pardi, L.; Kesselman, J. M.; Gantzel, P. K.; Chadha, R. K.; Gatteschi, D.; Harvey, D. F.; Hendrickson, D. N. *J. Am. Chem. Soc.* **1993**, *115*, 12483.

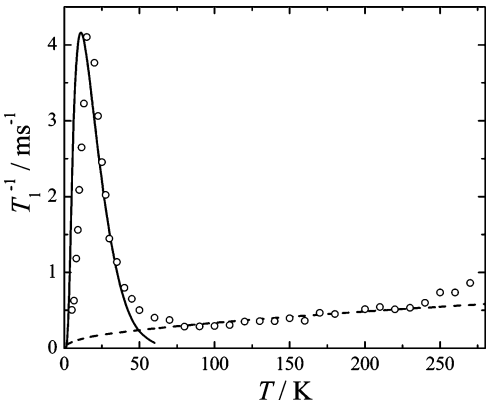

Figure 7. ^{1}H T_1 spin−lattice relaxation time of complex **2** as a function of temperature (the open circles represent the experimental data, the dashed line shows the temperature dependence of $\chi_M T$ in arbitrary units, and the solid line represents the fit to the experimental data according to eq 5).

$(OH)_2(O_2CMe)_{10}(hep)_2]$ [hep$^-$ = anion of 2-(2-hydroxyethyl)pyridine] and $[Fe_6O_2(OH)_2(O_2CMe)_{10}L_2]$ [L = 2-(N-methylimidazol-2-yl)-2-hydroxypropane] with identical coupling schemes proved to exhibit $S = 5$ and 0 ground states, respectively, because of differences in the relative coupling strengths. In the case of a prismatic Fe_6 cluster,[30] an $S = 1$ ground state was found to be stabilized, whereas examples of other Fe^{III}_6 complexes with $S = 5$ ground states are mentioned in ref 28. In this respect, complex **2** is a new example of a spin-coupling scheme, which leads to an $S = 0$ ground state because of its particular coupling features.

Solid-State NMR Studies. T_1 spin−lattice relaxation in paramagnetic and magnetic materials is a powerful tool to investigate the electron-spin dynamics of the system because the nuclei under investigation probe the fluctuating local magnetic fields induced at the nuclear sites through the hyperfine interaction.

The ^{1}H T_1 spin−lattice relaxation time of complex **2** was measured at a frequency of 200.145 MHz between room and liquid-helium temperatures. The nuclear relaxation rate $1/T_1$ as a function of temperature is shown in Figure 7. At high temperatures, $1/T_1$ exhibits a weak temperature dependence, while at low temperatures, a peak appears at ∼15 K. The appearance of a peak in $1/T_1$ at a temperature on the order of the magnetic exchange constant J/k_B has been frequently encountered in previous ^{1}H NMR studies of molecular clusters and rings.[31]

In particular, at high temperatures ($k_BT \gg J$), the magnetic moments in the cluster are weakly correlated and the system behaves like a paramagnet at high temperatures. In this limit, the spin dynamics is dominated by the behavior of the static response function, and it can be shown[32] that in this limit $1/T_1 \sim \chi_M T$, where χ_M is the uniform static susceptibility.

This proportionality is shown in Figure 7, where the dashed line shows the temperature dependence of $\chi_M T$ in arbitrary units.

At lower temperatures and particularly when the temperature is comparable to the magnetic exchange interaction J ($k_BT \approx J$), there is a growing of strong correlations in the fluctuations of the magnetic moments of the molecule. These correlations manifest themselves as an enhancement of the relaxation rate $1/T_1$ at a temperature on the order of the magnetic exchange constant J/k_B. This behavior is similar to the critical enhancement of relaxation in 3D magnetic systems at the transition temperature to long-range magnetic order. In molecular clusters, because of the finite size of the spin system, the low-lying energy states are well separated among themselves, and in this temperature range, the spin dynamics is governed by magnetic excitations between the ground state and the next excited state separated by an energy difference Δ. The appearance of the NMR $1/T_1$ peak can be explained with the use of a semiphenomenological model used in previous NMR studies in molecular rings.[31b,33] In particular, in this approach, the nuclear relaxation rate $1/T_1$ has contributions proportional to the probability of occupation of the different energy levels. The first contribution comes from the first excited state $\exp(-\Delta/k_BT)$ weighted by the sum of all of the energy states (the partition function), and the second contribution comes from the remaining states approximated by a continuum. Indeed, because the first excited states are 1.0 cm^{-1} ($S = 1$) and 10.0 cm^{-1} ($S = 2$) higher than the ground state, as obtained from the susceptibility data, it is expected that the nuclear relaxation rate will probe the energy difference $\Delta = 10$ cm^{-1} = 14.4 K (with the energy difference of 1 cm^{-1} being too small to be detected by NMR), and this is clearly demonstrated by the experimental NMR peak at ∼15 K (Figure 7). According to this simplified model, the expression for the NMR relaxation can be written as

$$\frac{1}{T_1} = C \exp\left(-\frac{\Delta}{k_BT}\right) Z^{-1} \qquad (5)$$

where $Z = \int_\infty^0 D(E) \exp(-E/k_BT)\, dE$ is the partition function, $D(E)$ is the distribution of energy levels, and C is a constant.

The experimental $1/T_1$ data have been fitted to eq 5 using $\Delta = 15$ K and assuming a Gaussian distribution for the continuum of the remaining states with a mean energy of 1200 K and a width of 220 K. The fit is shown as a solid curve in Figure 7, and it can be seen that it describes adequately the experimental data.

Therefore, NMR relaxation data have been used to probe the nature of the low-lying states and in particular the energy separation between them, and the results are in accordance with the susceptibility data.

Conclusions

Further investigation of the $Fe^{III}/PhCO_2^-/salox^{2-}$ reaction system has provided conclusions on certain aspects of its chemistry. Specifically, the use of weakly coordinating MeCN as the solvent led to two hexanuclear complexes [Fe_6-

(30) Shweky, I.; Pence, L. E.; Papaefthymiou, G. C.; Sessoli, R.; Bino, J. A.; Lippard, S. J. *J. Am. Chem. Soc.* **1997**, *119*, 1037.
(31) (a) Lascialfari, A.; Jang, Z. H.; Borsa, F.; Gatteschi, D.; Cornia, A. *J. Appl. Phys.* **1998**, *83*, 6946. (b) Lascialfari, A.; Gatteschi, D.; Borsa, F.; Cornia, A. *Phys. Rev. B* **1997**, *55*, 14341.
(32) Moriya, T. *Prog. Theor. Phys.* **1962**, *28*, 371.
(33) Fardis, M.; Diamantopoulos, G.; Karayianni, M.; Papavassiliou, G.; Tangoulis, V.; Konsta, A. S. *Phys. Rev. B* **2001**, *65*, 14412.

$(\mu_3\text{-O})_2(O_2CPh)_{10}(salox)_2(L)_2]\cdot x MeCN\cdot y H_2O$ [L = $MeCONH_2$, $x = 6$, $y = 0$ (**1**); L = H_2O, $x = 2$, $y = 3$ (**2**)], which can be regarded as dimers of trimers. Their synthesis has been achieved (i) by the $Fe^{III}/PhCO_2^-/H_2$salox reaction mixture in MeCN, (ii) by the reaction between "basic iron benzoate" and H_2salox in MeCN, and (iii) by recrystallization of the previously characterized trinuclear precursor complexes **III** and **IV** in MeCN, thus exploring the parameter space of this reaction system. On the other hand, the use of strongly coordinating alcoholic solvents stabilizes the respective trinuclear complexes **III** and **IV**. Both **1** and **2** contain the $[Fe_6(\mu_3\text{-O})_2(\mu_2\text{-OR})_2]^{12+}$ core, whose topology consists of six Fe^{III} ions arranged as two centrosymmetrically related $[Fe_3(\mu_3\text{-O})]$ subunits bridged by two oximato O atoms (O1 and O1′). Mössbauer spectra of **2** revealed that, as in the case of the trinuclear N/O-coordinated complexes **III** and **IV**, the primary factor influencing the quadrupole splittings is the donor atom homogeneity of the coordination sphere. It was thus possible to clearly distinguish between sites possessing O_6 and O_5N coordination spheres. For the interpretation of the magnetic susceptibility data, a model involving four different exchange coupling constants was required, leading to an $S = 0$ ground state. The first excited states were found to be only 1.0 cm^{-1} ($S = 1$) and 10.0 cm^{-1} ($S = 2$) higher than the ground state, a fact that has been confirmed by the presence of a significant enhancement of the $1/T_1$ NMR relaxation rate at ~15 K attributed to the energy difference between the ground and the $S = 2$ energy states.

Acknowledgment. We thank the Greek General Secretariat of Research and Technology for support within the frame of the Competitiveness EPAN 2000−2006, Centers of Excellence #25. A.K.B. thanks the Greek State Scholarship Foundation (IKY) for support through a postdoctoral grant.

Supporting Information Available: X-ray crystal crystallographic files, in CIF format, for **1** and **2**, as well as a figure of the polymeric chains of **1** formed by H-bonding interactions, a table with selected bond distances and angles in compound **1**, and the energy level plot for **2**. This material is available free of charge via the Internet at http://pubs.acs.org.

IC051945Q